

# Accepted Manuscript

A comparative study of the electronic spectra, fluorescence quantum yields, cyclic voltammograms and theoretical calculations of phenanthrene-type benzodifurans

Naoto Hayashi, Yoko Saito, Xiaoxi Zhou, Junro Yoshino, Hiroyuki Higuchi, Toshiki Mutai



PII: S0040-4020(16)30406-9

DOI: [10.1016/j.tet.2016.05.019](https://doi.org/10.1016/j.tet.2016.05.019)

Reference: TET 27746

To appear in: *Tetrahedron*

Received Date: 9 March 2016

Revised Date: 6 May 2016

Accepted Date: 9 May 2016

Please cite this article as: Hayashi N, Saito Y, Zhou X, Yoshino J, Higuchi H, Mutai T, A comparative study of the electronic spectra, fluorescence quantum yields, cyclic voltammograms and theoretical calculations of phenanthrene-type benzodifurans, *Tetrahedron* (2016), doi: 10.1016/j.tet.2016.05.019.

This is a PDF file of an unedited manuscript that has been accepted for publication. As a service to our customers we are providing this early version of the manuscript. The manuscript will undergo copyediting, typesetting, and review of the resulting proof before it is published in its final form. Please note that during the production process errors may be discovered which could affect the content, and all legal disclaimers that apply to the journal pertain.

## Graphical Abstract

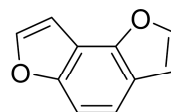
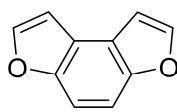
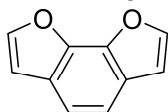
To create your abstract, type over the instructions in the template box below.  
Fonts or abstract dimensions should not be changed or altered.

**A comparative study of the electronic spectra, fluorescence quantum yields, cyclic voltammograms and theoretical calculations of phenanthrene-type benzodifurans**

Leave this area blank for abstract info.

Naoto Hayashi<sup>a,\*</sup>, Yoko Saito<sup>a</sup>, Xiaoxi Zhou<sup>a</sup>, Junro Yoshino<sup>a</sup>, Hiroyuki Higuchi<sup>a</sup> and Toshiki Mutai<sup>b,\*</sup>

<sup>a</sup>Graduate School of Science and Engineering, University of Toyama, Gofuku, Toyama 930-8555, Japan, <sup>b</sup>Institute of Industrial Science, The University of Tokyo, Komaba, Meguro-ku, Tokyo 153-8505, Japan



ACCEPTED MANUSCRIPT



Tetrahedron  
journal homepage: www.elsevier.com



## A comparative study of the electronic spectra, fluorescence quantum yields, cyclic voltammograms and theoretical calculations of phenanthrene-type benzodifurans

Naoto Hayashi<sup>a, \*</sup>, Yoko Saito<sup>a</sup>, Xiaoxi Zhou<sup>a</sup>, Junro Yoshino<sup>a</sup>, Hiroyuki Higuchi<sup>a</sup> and Toshiki Mutai<sup>b, \*</sup>

<sup>a</sup>Graduate School of Science and Engineering, University of Toyama, Gofuku, Toyama 930-8555, Japan

<sup>b</sup>Institute of Industrial Science, The University of Tokyo, Komaba, Meguro-ku, Tokyo 153-8505, Japan

### ARTICLE INFO

#### Article history:

Received

Received in revised form

Accepted

Available online

#### Keywords:

Benzodifurans

Oxidation potentials

Fluorescence quantum yields

HOMO/LUMO energy levels

### ABSTRACT

Three isomeric difuran analogues of phenanthrene, including benzo[1,2-*b*;6,5-*b'*]difuran (**3O**), benzo[1,2-*b*;4,3-*b'*]difuran (**4O**) and benzo[1,2-*b*;3,4-*b'*]difuran (**5O**) have prepared and their properties investigated systematically. Compared with benzo[1,2-*b*;4,5-*b'*]difuran (**1O**) and benzo[1,2-*b*;5,4-*b'*]difuran (**2O**), there were pronounced differences in the fluorescence quantum yields of **3O–5O**. Consideration of the absorption and fluorescence spectra, cyclic voltammograms and B3LYP/6-31G(d,p) calculations revealed that **4O** had the highest electron-donating/accepting characteristics of all of the compounds prepared in this study. The lower electron-donating/accepting properties of **5O** were attributed to the shorter chain length of its  $\pi$ -conjugated system. The unexpectedly high electron-donating and low electron-accepting properties of **3O** were attributed to changes in the radical cationic and anionic states, respectively. The energy levels of the highest occupied and lowest unoccupied molecular orbitals of the thiophene and selenophene analogues of **3O–5O** have also been calculated, and their relative energies explained in a similar manner.

2009 Elsevier Ltd. All rights reserved.

\* Corresponding author. Tel.: +81-76-445-6613; fax: +81-76-445-6549; e-mail: nhayashi@sci.u-toyama.ac.jp (Naoto Hayashi)

\* Corresponding author. Tel.: +81 3 5452 6098 (ext. 57936); fax: +81 3 5452 6353; e-mail: mutai@iis.u-tokyo.ac.jp (Toshiki Mutai)

## 1. Introduction

Fused heteroaromatic compounds have attracted considerable interest from researchers working in the field of organic electronic materials chemistry.<sup>1</sup> In contrast to fused aromatic hydrocarbons, fused heteroaromatic compounds can exist as structural isomers with respect to the direction of the fused heteroaromatic rings.<sup>2</sup> Although these isomers are alike in terms of their molecular structure, their intrinsic properties, assembly structures and intermolecular electronic interactions can vary considerably. The appropriate use of these isomers and isomeric moieties can therefore provide interesting opportunities to tune the molecular and/or aggregation structures derived from these fused heteroaromatic compounds to generate unique materials with specific properties.

Fused-thiophene compounds are among the most frequently and extensively studied of all the fused heteroaromatic compounds reported in the literature,<sup>3</sup> because of their highly electron-donating character, chemical stability and ability to form specific intermolecular interactions such as S...S bonds.<sup>4-7</sup> Benzodithiophenes (BDTs) are one of the simplest fused-thiophene systems capable of existing as structural isomers with respect to the direction of their fused thiophene rings. Furthermore, the BDT derivatives **1S–5S** (Chart 1) have been investigated much more extensively than any other directional isomers because of their stability and availability. BDTs **1S** and **2S** are isomers of each other with respect to the direction of their two thiophene moieties. Furthermore, the structures of **1S** and **2S** are isoelectronic with anthracene, which is why they are sometimes referred to as anthracene-type BDTs. Although BDTs **3S**, **4S** and **5S** can exist as different isomeric structures in the same way as **1S** and **2S**, they are isoelectronic with phenanthrene, and are therefore referred to as phenanthrene-type BDTs. BDTs **1S–5S** have been used to develop a wide variety of organic

electronic materials, such as organic field-effect transistors (OFETs)<sup>8-10</sup> and photovoltaics (PVs).<sup>11,12</sup> A comparison of these materials revealed that their physical and electronic properties varied considerably in some cases and only slightly in others, depending on the differences in the electronic characteristics of the different BDT moieties. Moreover, Müllen and the co-workers reported differences in the OFET behaviors of isomeric copolymers consisting of **1S–5S** moieties, which they explained in terms of their electronic characteristic, as well as the shape of the polymeric molecules.<sup>13</sup>

Several fused-furan compounds have also been studied in terms of the differences in the properties of their structural isomers.<sup>14</sup> In contrast to fused-thiophene compounds, fused-furan compounds likely form weaker intermolecular electronic interactions because they cannot form S...S interactions. For this reason, fused-furan compounds tend to have poorer OFET properties (i.e., small mobility). However, the lack of sulfur atoms in fused-furan systems can enhance their fluorescence quantum yields compared with their fused-thiophene counterparts because they do not experience a heavy atom effect. Based on the differences in the intrinsic properties of fused-furan and fused-thiophene compounds, it should be possible to use these systems to develop new materials with specifically tailored properties. Unfortunately, however, there have been very few studies aimed at developing a thorough understanding of the differences between these compounds, which currently remain unclear.

Benzodifurans (BDFs) are the furan analogue of BDTs. In a similar manner to BDTs, the BDF derivatives **10–50** have also been studied extensively.<sup>15-19</sup> Given that the behaviors of these derivatives are largely dependent on the intrinsic properties of their BDF moieties, it is important to have a thorough understanding of the characteristics of the BDF moieties themselves. With this in mind, we previously conducted a series of spectral, electrochemical and theoretical studies on the anthracene-type BDFs **10** and **20**.<sup>20</sup> It is noteworthy that the electron-donating abilities of **10** and **20** were found to be very different to those of the corresponding BDTs **1S** and **2S**.<sup>21</sup> Furthermore, the fluorescence quantum yields of **10** and **20** were virtually identical, whereas those of **1S** and **2S** were very different. The differences in these results could be attributed to the unique properties of BDFs compared with BDTs. Notably, however, there have been no systematic studies on the properties of the phenanthrene-type BDFs **30–50**, despite the fact that a large number of compounds have been synthesized consisting of **30–50** moieties and their properties examined.<sup>22-26</sup> For this reason, discussions pertaining to the observed properties of these material in the context of their individual BDF moieties have been limited in most cases. To address this issue, we have synthesized **30–50** and systematically characterized these compounds spectroscopically, electrochemically and theoretically by comparing them to the isomeric compounds **10** and **20**, as well as their thiophene (**1S–5S**) and selenophene (**1Se–5Se**) analogues.

## 2. Results

## 2.1. Synthesis

Phenanthrene-type BDFs can be synthesized in a variety of different ways,<sup>27-33</sup> and the BDFs prepared in the current study (**30–50**) were synthesized in a similar manner to **10** and **20**, as depicted in Scheme 1.

For the synthesis of **30**, 3,6-diiodocatechol (**6**) was initially diesterified to give **7**, which was subjected to a Sonogashira coupling<sup>34,35</sup> with trimethylsilylacetylene (TMSA) to afford **8**.

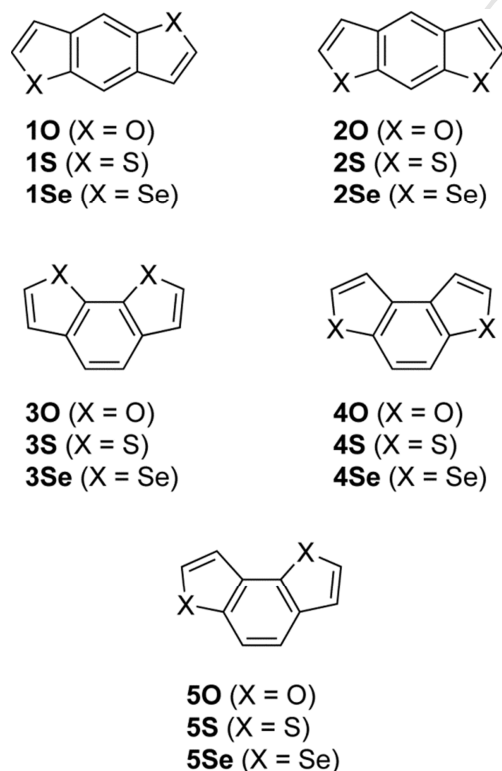
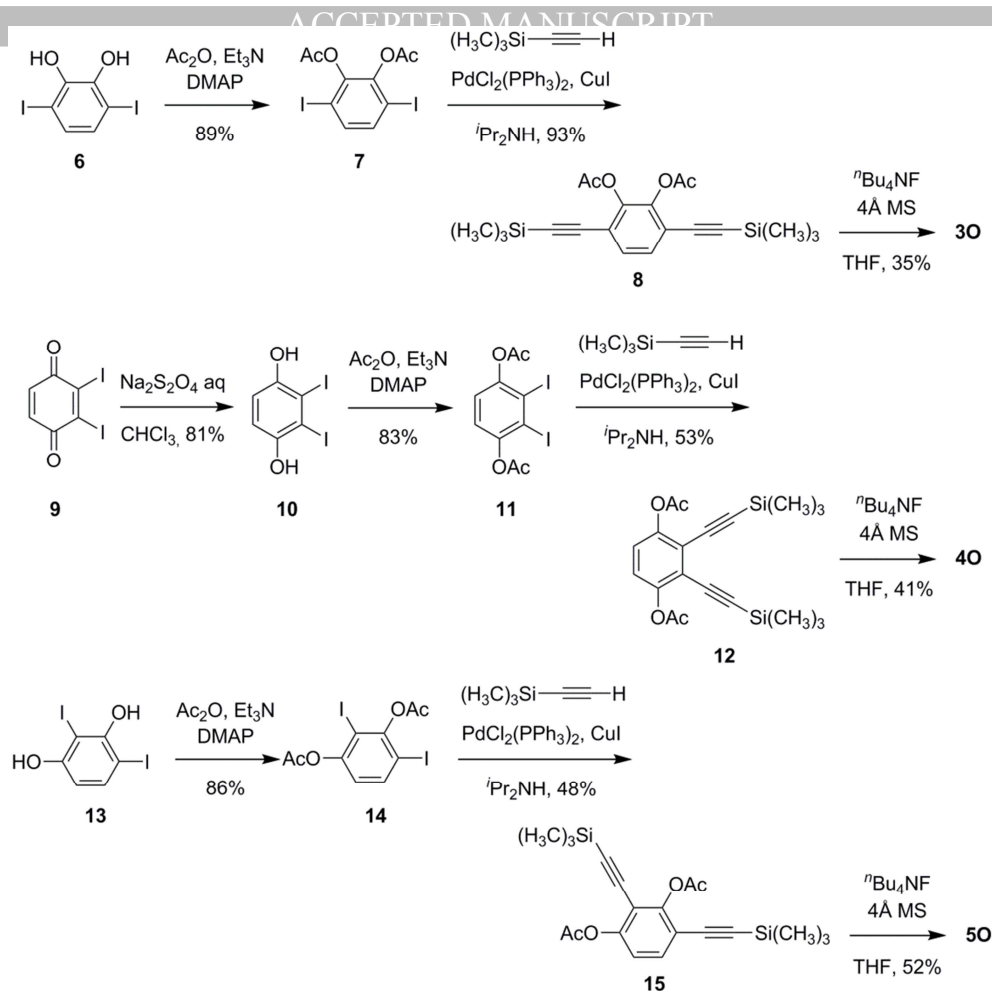


Chart 1.



Scheme 1.

Compound **8** was subsequently subjected to sequential cyclization and desilylation reactions using tetrabutylammonium fluoride and 4 Å molecular sieves<sup>36</sup> to yield the target compound. Isomers **40** and **50** were obtained in a similar manner using **10** (prepared from **9**) and **13**, respectively. It is noteworthy that the yield for the final step in the synthesis of **50** was comparable to those of **30** and **40**.

## 2.2. Electronic absorption spectra

Kellogg and co-workers previously reported the electronic absorption spectra of **40**, **4S** and **5S** in cyclohexane.<sup>31</sup> These results revealed that the longest-wavelength  $\pi-\pi^*$  absorption peaks of **40** and **4S** were observed at 294 and 317 nm, respectively (Table 1). Notably, the longest-wavelength  $\pi-\pi^*$  absorption peak of **5S** had a slightly higher bathochromic shift than that of **4S** at 320 nm. The molar absorption coefficients ( $\epsilon$ ) of the longest-wavelength absorption peaks of **40**, **4S** and **5S** were similar. In the present study, we not only measured the electronic absorption spectra of **30** and **50** but also measured those of **40** and phenanthrene for a fair comparison.

As shown in Figure 1, there were considerable differences in the shapes of the longest-wavelength absorption bands in the electronic absorption spectra of **30–50**. The longest-wavelength absorption peak of **40** appeared at  $\lambda_{\text{peak}} = 294$  nm, which was in agreement with the value reported by Kellogg and the co-workers, while that of **50** was observed at  $\lambda_{\text{peak}} = 297$  nm. The bathochromic shifts of **4S** and **5S** were also very similar. In contrast, the hypsochromic shift of **30** was observed at its longest-wavelength absorption peak ( $\lambda_{\text{peak}} = 284$  nm). The  $\log \epsilon$

values of **40** (3.36) and **50** (3.26) were similar, whereas the value for **30** (2.84) was much lower. No significant changes were observed in the spectra of these compounds when they were run in ethanol (Figure S1), which indicated that these behaviors could be attributed to the intrinsic properties of **30–50** rather than a solvent effect.

## 2.3. Fluorescence spectra

The fluorescence spectra of **30–50** and phenanthrene are also shown in Figure 1. The spectra of **30–50** all contained three principal peaks (or shoulder), although the intensity ratios of these peaks varied for the different compounds. Notably, the Stokes shifts of **30–50** were much smaller (10, 1 and 0 nm, respectively) than that of phenanthrene (52 nm). No discernible differences were observed in the shapes of these spectra when they were run in ethanol (Figure S1). In contrast to the absorption spectra, large differences were observed in the peak wavelengths of **30–50** compared with that of phenanthrene, because of the different Stokes shifts. The fluorescence quantum yields ( $\Phi_{\text{F}}$ ) of **30–50** were 0.03, 0.74 and 0.19, respectively.

## 2.4. Cyclic voltammograms

The cyclic voltammograms of **30–50** were obtained in acetonitrile. All three cyclic voltammograms contained a similar irreversible one-electron oxidative wave, as shown in Figure 2. The onset values for the oxidative waves ( $E_{\text{a}}^{\text{onset}}$ ) in compounds **30** and **40** were identical, whilst there was a pronounced positive shift in the onset value of **50**. It is noteworthy that the gaps between  $E_{\text{a}}^{\text{onset}}(\mathbf{30})$  and  $E_{\text{a}}^{\text{onset}}(\mathbf{50})$  ( $\Delta E_{\text{a}}^{\text{onset}} = 0.10$  V),  $E_{\text{a}}^{\text{onset}}(\mathbf{40})$  and  $E_{\text{a}}^{\text{onset}}(\mathbf{50})$  (0.07 V) and  $E_{\text{a}}^{\text{onset}}(\mathbf{10})$  and  $E_{\text{a}}^{\text{onset}}(\mathbf{20})$

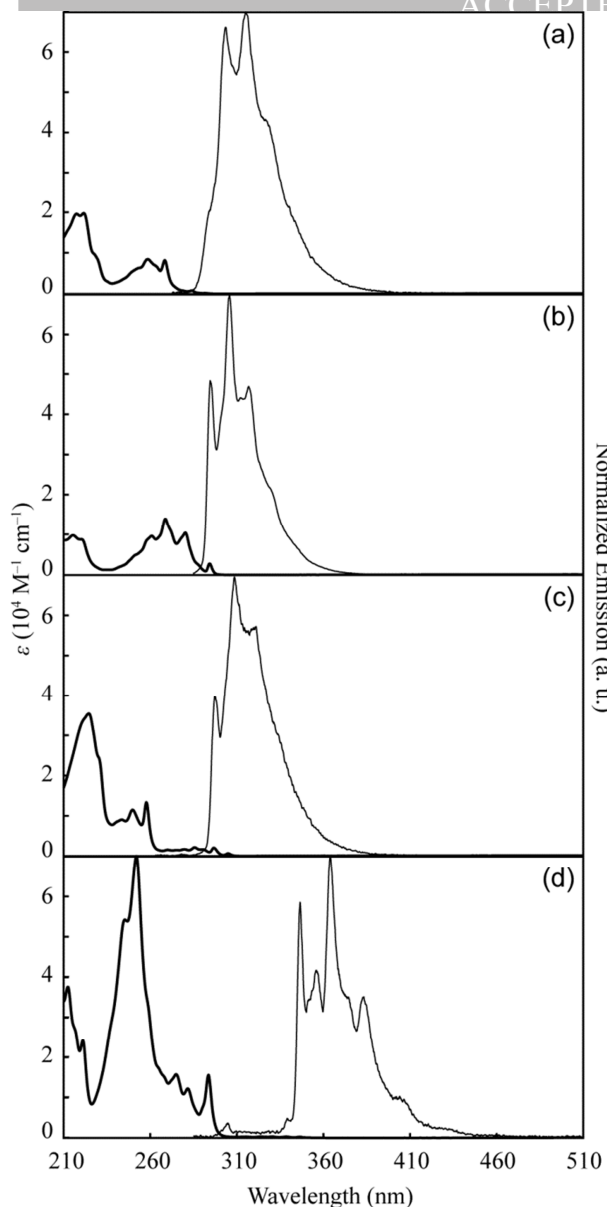


**Figure 1.** Electronic absorption spectra (thick lines) and fluorescence spectra (thin lines) of **30** (a), **40** (b), **50** (c) and phenanthrene (d) in cyclohexane.

(0.08 V) were very similar. On the other hand, no reductive waves were observed under our experimental conditions.

### 2.5. Theoretical calculations

Hybrid DFT calculations were performed at the B3LYP/6-31G(d,p) level to develop a deeper understanding of the different characteristics of compounds **30–50**. Compounds **3S–5S** and **3Se–5Se** were also studied in the same way for comparison. The results of the calculation are shown in Figure 3 and Table 2.

We initially compared the energy levels of the highest occupied molecular orbital (HOMO),  $E_{\text{HOMO}}$ , of the isomeric compounds **30–50**, **3S–5S** and **3Se–5Se**. The results revealed that  $E_{\text{HOMO}}(\mathbf{40})$  was higher than  $E_{\text{HOMO}}(\mathbf{50})$ . Furthermore,  $E_{\text{HOMO}}(\mathbf{4S})$  and  $E_{\text{HOMO}}(\mathbf{4Se})$  were higher than  $E_{\text{HOMO}}(\mathbf{5S})$  and  $E_{\text{HOMO}}(\mathbf{5Se})$ , respectively. However,  $E_{\text{HOMO}}(\mathbf{30})$  was similar to

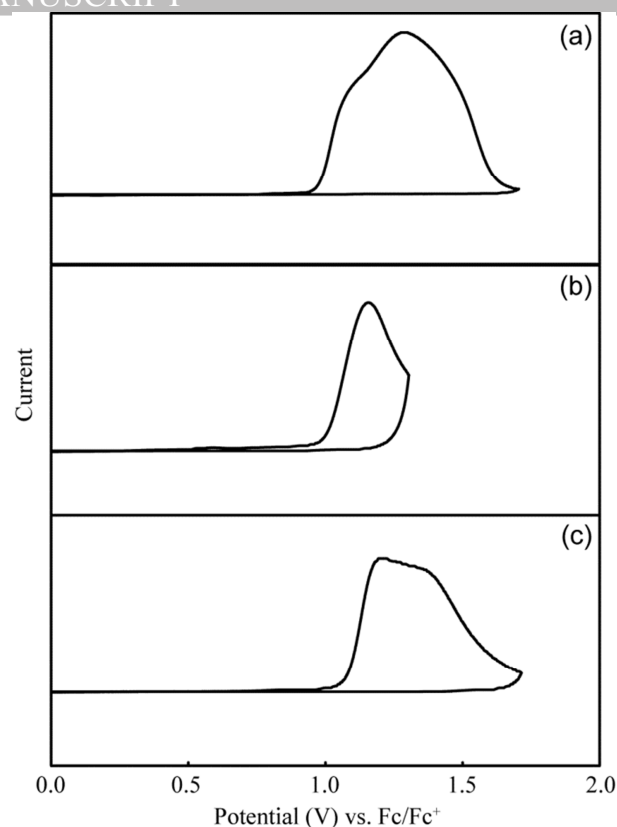


**Figure 2.** Cyclic voltammograms of **30** (a), **40** (b) and **50** (c) in  $\text{CH}_3\text{CN}$  at a scan rate of  $100 \text{ mV s}^{-1}$ .

$E_{\text{HOMO}}(\mathbf{40})$ , whereas  $E_{\text{HOMO}}(\mathbf{3S})$  and  $E_{\text{HOMO}}(\mathbf{3Se})$  were lower than  $E_{\text{HOMO}}(\mathbf{4S})$  and  $E_{\text{HOMO}}(\mathbf{4Se})$ , respectively.

A comparison of the energy levels of the lowest unoccupied molecular orbitals (LUMO),  $E_{\text{LUMO}}$ , of these compounds revealed that  $E_{\text{LUMO}}(\mathbf{4X})$  was much lower than  $E_{\text{LUMO}}(\mathbf{5X})$ , irrespective of the identity of **X** (i.e., **X** = **O**, **S** or **Se**). In contrast,  $E_{\text{LUMO}}(\mathbf{30})$  was much higher than  $E_{\text{LUMO}}(\mathbf{40})$  and  $E_{\text{LUMO}}(\mathbf{50})$ . Although  $E_{\text{LUMO}}(\mathbf{3S})$  was slightly higher than  $E_{\text{LUMO}}(\mathbf{4S})$  and much higher than  $E_{\text{LUMO}}(\mathbf{3Se})$ , it was lower than  $E_{\text{LUMO}}(\mathbf{4Se})$ .

We subsequently compared the HOMO and LUMO energy levels of the isoelectronic compounds, **30–3Se**, **40–4Se** and **50–5Se**, which only varied in terms of the nature of their chalcogen atoms. The results revealed that the fused-furan and fused-selenophene compounds had the highest and the lowest LUMO energy levels, respectively. The energy gaps between the fused-furan and fused-thiophene compounds (0.16–0.56 eV) were larger than those between the fused-thiophene and fused-selenophene compounds (0.04–0.14 eV). A similar trend was observed for a comparison of compounds **10–1Se**, where the LUMO energy levels decreased in the order of  $E_{\text{LUMO}}(\mathbf{10}) > E_{\text{LUMO}}(\mathbf{1S}) > E_{\text{LUMO}}(\mathbf{1Se})$ . However, the order of the LUMO energy levels for compounds **20–2Se** was slightly different as  $E_{\text{LUMO}}(\mathbf{20}) > E_{\text{LUMO}}(\mathbf{2Se}) > E_{\text{LUMO}}(\mathbf{2S})$ , with the furan-fused compound still acting as the strongest electron-accepter and the thiophene-fused and selenophene-fused compounds swapping places. Notably, the energy gaps were much larger between the fused-furan and fused-thiophene compounds (**10/1S**, 0.28 eV; **20/2S**, 0.16 eV) than they were between the fused-thiophene and fused-selenophene compounds (**1S/1Se**, 0.05 eV; **2S/2Se**, –0.04 eV).

In contrast to the LUMO energy levels of **3O–3Se**, **4O–4Se** and **5O–5Se**, the order of the HOMO energy levels was much more complicated. For example,  $E_{\text{HOMO}}(\mathbf{3O})$  was higher than  $E_{\text{HOMO}}(\mathbf{3S})$  and  $E_{\text{HOMO}}(\mathbf{3Se})$ , and  $E_{\text{HOMO}}(\mathbf{4O})$  was determined to be higher than  $E_{\text{HOMO}}(\mathbf{4S})$  and  $E_{\text{HOMO}}(\mathbf{4Se})$ . However,  $E_{\text{HOMO}}(\mathbf{5Se})$  was found to be the highest value for compounds **5O–5Se**. Furthermore, the energy gaps between the HOMO levels of the different compounds were smaller (0.01–0.09 eV) than the corresponding gaps between the LUMO energy levels. A comparison of the HOMO energy levels for compounds **3O–3Se**, **4O–4Se** and **5O–5Se** revealed that they were contrary to those of compounds **1O–1Se** and **2O–2Se**, in which the HOMO energy levels of the fused-furan and fused-selenophene compounds were the lowest and highest, respectively.

TD-DFT calculations were performed to analyze the electronic absorption spectra of the different compounds prepared in the current study. The  $S_0$ – $S_1$  absorptions (longest-wavelength absorptions) and  $S_0$ – $S_2$  absorptions of compounds **3O–5O** were assigned as shown in Table 3. Although considerable differences

were observed in the HOMO/LUMO energy gaps of these compounds, it was predicted that the  $S_0$ – $S_1$  transitions of **4O** and **5O** would give an identical  $\lambda_{\text{peak}}$  value. However, the oscillator strength ( $f$ ) of **4O** was much larger than that of **5O**. Compared with **4O** and **5O**, there was a slight hypsochromic shift in the  $S_0$ – $S_1$  transition of **3O** of 4 nm. It is noteworthy that  $f$  value of this transition was very small, whereas the  $f$  value for the  $S_0$ – $S_2$  transition of **3O** was large and around 11 nm shorter than those of the longest-wavelength absorptions of **4O** and **5O**. Consequently, the longest-wavelength absorption of **3O** was found to be hypsochromically shifted to a much greater extent than expected.

### 3. Discussion

#### 3.1. Synthesis

It was envisaged that the cyclization and desilylation of **15** to give **5O** would afford a low yield of the desired product because **15** could potentially proceed down three different cyclization

**Table 1.** Collection of spectroscopic properties and oxidation potentials for **3O–5O**, **4S** and **5S**.

	<b>3O</b>	<b>4O</b>	<b>5O</b>	<b>4S<sup>a</sup></b>	<b>5S<sup>a</sup></b>
$\lambda_{\text{max}}$ (log $\epsilon$ )	218(4.29), 222(4.30), 259(3.93), 267(3.80),284(2.84)	216(3.99), 261(3.98), 269(4.14), 281(4.00), 294(3.36)	225(4.54), 244(3.95), 250(4.05), 258(4.11), 270(3.15), 280(3.18), 286(3.29), 297(3.26)	219 (4.47), 234 sh (4.11), 248 sh (4.09), 252 (4.16), 257 (4.10), 268 (3.95), 277 (4.11), 288 (4.29), 300 (4.20), 317 (3.53)	205 (4.08), 223 (4.13), 248 sh (4.48), 255 (4.58), 275 (4.03), 286 (3.90), 296 (3.23), 307 (3.23), 315 (2.93), 320 (3.20)
$\lambda_{\text{F, max}}$	304, 315, 327(sh)	295, 306, 312, 317, 330(sh)	297, 308, 321	– <sup>f</sup>	– <sup>f</sup>
$\Phi_{\text{F}}^{\text{d}}$	0.03	0.74	0.19	– <sup>f</sup>	– <sup>f</sup>
$E_{\text{a}}^{\text{onset}} / \text{V}^{\text{e}}$	+0.98	+1.01	+1.08	– <sup>f</sup>	– <sup>f</sup>

<sup>a</sup>Ref. 31. <sup>b</sup>In cyclohexane. <sup>c</sup>Excitation wavelengths of 268, 280 and 258 nm for **3O**, **4O** and **5O**, respectively. <sup>d</sup>In EtOH. <sup>e</sup>Electrode; Pt (working), Pt (counter) and Ag/AgCl (reference). Supporting electrolyte *n*-Bu<sub>4</sub>NPF<sub>6</sub>. Solvent; CH<sub>3</sub>CN. Scan rate; 100 mV/s. Versus ferrocene/ferrocenium. *c* ~ 1 mmol/L. <sup>f</sup>Not reported.

**Table 2.** HOMO and LUMO energy levels (in eV) for **1O–5O**, **1S–5S** and **1Se–5Se** calculated using DFT at the B3LYP/6-31G(d,p) level.

	<b>1X<sup>a</sup></b>	<b>2X<sup>a</sup></b>	<b>3X</b>	<b>4X</b>	<b>5X</b>
[HOMO]					
<b>X = O</b>	–5.54	–5.70	–5.63	–5.63	–5.76
<b>X = S</b>	–5.48	–5.50	–5.76	–5.67	–5.78
<b>X = Se</b>	–5.42	–5.44	–5.74	–5.64	–5.71
[LUMO]					
<b>X = O</b>	–0.82	–0.70	–0.41	–0.71	–0.45
<b>X = S</b>	–1.10	–0.90	–0.97	–1.02	–0.81
<b>X = Se</b>	–1.15	–0.86	–1.11	–1.09	–0.90

<sup>a</sup>Ref. 20.

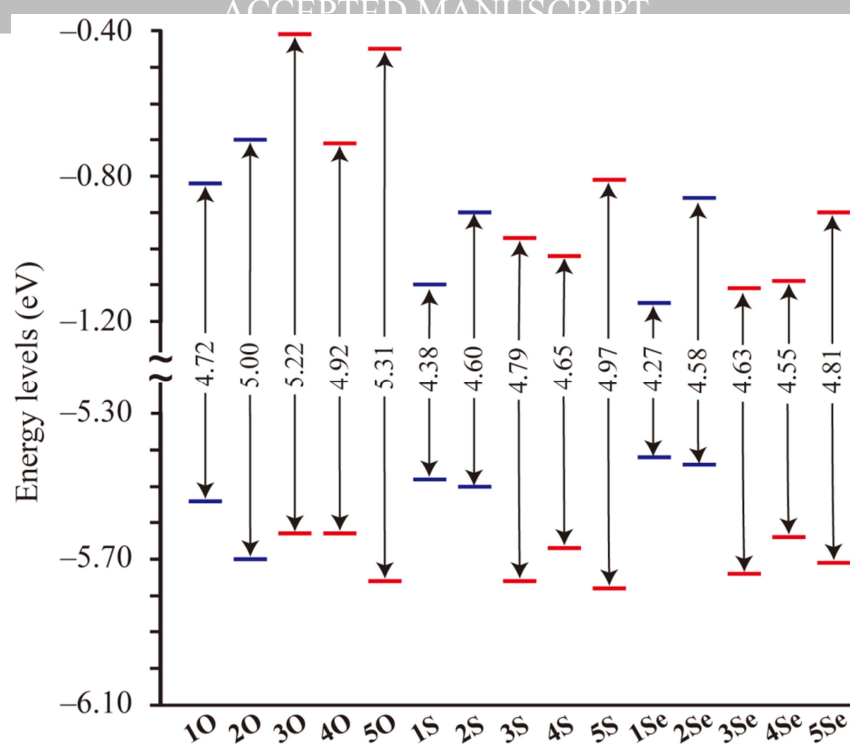


**Figure 3.** Diagram of the HOMO and LUMO energy levels of **1O–5O**, **1S–5S** and **1Se–5Se**, which were calculated using DFT at the B3LYP/6-31G(d,p) level.

pathways (i.e., path *a*, *b* and *c*). Whilst pathways *a* and *c* would provide access to the desired product **5O** pathway *b* would afford the undesired product **16** and/or its derivatives (Figure 4). However, the actual yield for this step was higher than expected, and comparable with those of the reactions to give **3O** and **4O**. The success of this reaction was attributed to the first saponification occurring at the less sterically crowded acetoxy group (at the 1-position), followed by the formation of the furan ring via pathway *a* before the second saponification reaction. The validity of this mechanism was supported by the fact that none of the undesired product **16** was detected in the reaction mixture.

### 3.2. Electronic absorption spectra

The longest-wavelength absorption peaks in the electronic

absorption spectra of compounds **3O–5O** appeared in a shorter-wavelength region (284–297 nm) compared with those of compounds **1O** and **2O** (302–307 nm). Similar hypsochromic shifts were also observed in the spectra of the analogous hydrocarbon compounds, phenanthrene and anthracene. The  $\epsilon$  values varied considerably for the longest-wavelength absorption peaks of **3O–5O**, whereas those of **1O** and **2O** were virtually identical. No discernible differences were observed in the peak positions ( $\Delta\lambda_{\text{peak}} < 10$  nm) based on a comparison of the  $\lambda_{\text{peak}}$  value of phenanthrene with those of **3O–5O**. However, this result was contrary to the large  $\Delta\lambda_{\text{peak}}$  values observed for **1O** and **2O** compared with anthracene. Furthermore, there was a considerable difference in the  $\lambda_{\text{peak}}$  values of **4O** and **4S** ( $\Delta\lambda_{\text{peak}} = 22$  nm), as well as those of **5O** and **5S** ( $\Delta\lambda_{\text{peak}} = 23$  nm).

**Table 3.** Assignments, wavelengths and oscillator strengths (*f*) of the  $S_0-S_1$  and  $S_0-S_2$  transitions of **3O**, **4O** and **5O**, which were obtained by TD-DFT calculations at the B3LYP/6-31G(d) level.

transitions	<b>3O</b>	<b>4O</b>	<b>5O</b>
$S_0-S_1$	-0.49 (HOMO - 1 $\rightarrow$ LUMO) + 0.51 (HOMO $\rightarrow$ LUMO + 1)	-0.17 (HOMO - 1 $\rightarrow$ LUMO + 2) + 0.63 (HOMO $\rightarrow$ LUMO)	0.52 (HOMO - 1 $\rightarrow$ LUMO) + 0.11 (HOMO - 1 $\rightarrow$ LUMO + 1) + 0.26 (HOMO $\rightarrow$ LUMO) + 0.37 (HOMO $\rightarrow$ LUMO + 1)
wavelength (nm), <i>f</i>	260, 0.002	264, 0.317	264, 0.017
$S_0-S_2$	0.26 (HOMO - 1 $\rightarrow$ LUMO + 1) + 0.61 (HOMO $\rightarrow$ LUMO)	0.59 (HOMO - 1 $\rightarrow$ LUMO) + 0.33 (HOMO $\rightarrow$ LUMO + 1) + 0.18 (HOMO $\rightarrow$ LUMO + 2)	-0.22 (HOMO - 1 $\rightarrow$ LUMO) + 0.19 (HOMO - 1 $\rightarrow$ LUMO + 1) + 0.56 (HOMO $\rightarrow$ LUMO) + 0.17 (HOMO $\rightarrow$ LUMO + 1)
wavelength (nm), <i>f</i>	253, 0.196	258, 0.039	248, 0.116

oxidation potentials, they did show quite similar qualitative behaviors. However, it is not possible to discuss the reduction potentials in the same context because they cannot be measured directly by cyclic voltammetry. It was envisaged that the half-wave reduction potentials of **30–50** would be in the range of  $-4.1$  to  $-4.4$  V (vs Fc/Fc<sup>+</sup>), which would be outside of the standard potential window. Furthermore, it was not possible to estimate these values based on the oxidation potentials and optical gaps measured in their electronic spectra, because the S<sub>0</sub>–S<sub>1</sub> transition energies of **30–50** could not be related to their HOMO/LUMO energy gaps in a simple manner, as shown in Table 3. For this reason, it was only possible to estimate the electron-accepting characteristics of **30–50** using theoretical calculations.

There were significant differences in the  $\Phi_F$  values of the compounds belonging to series **30–50**. For example, compounds **30** and **40** were found to be weakly and intensely fluorescent, respectively, whereas the fluorescence of **50** was intermediate. These results contrasted with the  $\Phi_F$  values observed for **10** and **20**, which were almost identical (0.43 and 0.41, respectively). In most cases, there are discernible differences in the  $\Phi_F$  values of the different directional isomers of fused heteroaromatic rings.<sup>20,21,37,38</sup> In this case, compounds **30–50** exhibited typical behaviors, whereas **10** and **20** acted as an exception to this general rule. Comparing **30–50**, the compound bearing larger  $\Phi_F$  value has the larger oscillator strength ( $f$ ) in the S<sub>0</sub>–S<sub>1</sub> transition. This should indicate that the larger  $\Phi_F$  value is due to significant overlap of the involved orbitals in the S<sub>0</sub>–S<sub>1</sub> transition. Phenanthrene-type fused aromatic compounds generally have larger  $\Phi_F$  values than their anthracene-type isomers.<sup>39</sup> However, there were no obvious trends between the  $\Phi_F$  values of compounds **10–50**. For example, the  $\Phi_F$  value of **40** was larger than those of **10** and **20**, while those of **30** and **50** were smaller. A comparison of the  $\Phi_F$  value of the isoelectronic hydrocarbon phenanthrene ( $\Phi_F = 0.13$ ),<sup>40</sup> with those of **30–50**, revealed that the value of **30** was smaller, whereas those of **40** and **50** were larger. In contrast, compounds **10** and **20** both had larger  $\Phi_F$  values than anthracene ( $\Phi_F = 0.27$ ).<sup>40</sup>

### 3.4. Evaluation of the experimental and theoretical results for compounds **30–50**

As shown in Table 1, the  $E_a^{\text{onset}}$  values of **30**, **40** and **50** were determined to be +0.98, +1.01 and +1.08 V, respectively, while their half-wave oxidation potentials ( $E_{1/2}$  vs Fc/Fc<sup>+</sup>) were estimated to be +0.83, +0.83 and +0.96 V, respectively, using the equation  $E_{1/2} = -(E_{\text{HOMO}} + 4.8)$ .<sup>41</sup> Although these values cannot be compared qualitatively because of the irreversibility of the

### 3.5. The HOMO/LUMO energy levels

It is generally accepted that the canonical structure of an isomeric compound with the longest series of alternating single and double (or triple) bonds should have the most efficiently extended  $\pi$ -conjugated system and therefore exhibit greater electron-donating/electron-accepting characteristics (i.e., higher  $E_{\text{HOMO}}$  and lower  $E_{\text{LUMO}}$  levels, respectively). Indeed, different  $E_a^{\text{onset}}$  values have been explained in this manner for several isomeric compounds, including **10** and **20**, isomeric thienobisbenzothiophenes<sup>21,42</sup> and isomeric tetrathienoanthracenes.<sup>38</sup> Based on this guideline, the  $\pi$ -systems for the compounds in the current study would be extended in the order of **50** < **30** < **40**, because the longest series of alternating single and double bonds would be consistent with the structures depicted in Figure 5. However, this expected order was inconsistent with the experimental and theoretical results. In fact, the observed oxidation potentials and calculated HOMO energy levels were of the order of  $E_{\text{HOMO}}(\mathbf{50}) < E_{\text{HOMO}}(\mathbf{30}) = E_{\text{HOMO}}(\mathbf{40})$ , whereas the LUMO energy levels were of the order of  $E_{\text{LUMO}}(\mathbf{30}) > E_{\text{LUMO}}(\mathbf{50}) > E_{\text{LUMO}}(\mathbf{40})$ .

This inconsistency can be explained by using canonical structures as follows. Although the theoretical description based on the molecular orbital theory is generally better than the explanation by means of the canonical structures, the latter one would be accepted more easily to the experimental researcher. The order of the HOMO and LUMO energy levels of a given series of isomeric molecules can be determined at a fundamental level based on the canonical structures with the longest series of alternating single and double bonds. Furthermore, we hypothesized that the energy levels could be raised or lowered to some extent by the stabilizing/destabilizing effects on the radical cationic or radical anionic states. According to the Koopmans' theorem,<sup>43</sup> when the HOMO energy level of a given molecule is high or the molecule itself has a strong electron-donating ability, the radical cation state should be highly stabilized (or vice versa). Alternatively, when the LUMO energy level of a given molecule is low, or the molecule itself has a strong electron-accepting ability, the radical anion state should be highly stabilized (or vice versa).

With regard to the HOMO energy levels of **30–50**, the  $E_{\text{HOMO}}(\mathbf{30})$  value was much higher than expected, most likely because of the stabilizing effect of the radical cation state of **30**, **30**<sup>+</sup>. Consideration of the resonance forms of **30**<sup>+</sup> revealed that canonical structure **I** (Figure 6) would make the greatest charge contribution to the overall structure, with the positive charge residing on the  $\alpha$  position of the furan ring and the unpaired electron on the  $\beta$  position. This form would be favored because the central benzene ring can be described as a complete Kekulé structure, with the unpaired electron being stabilized by a benzyl-type resonance, and the positive charge being stabilized through a resonance effect with the adjacent oxygen atom (see canonical

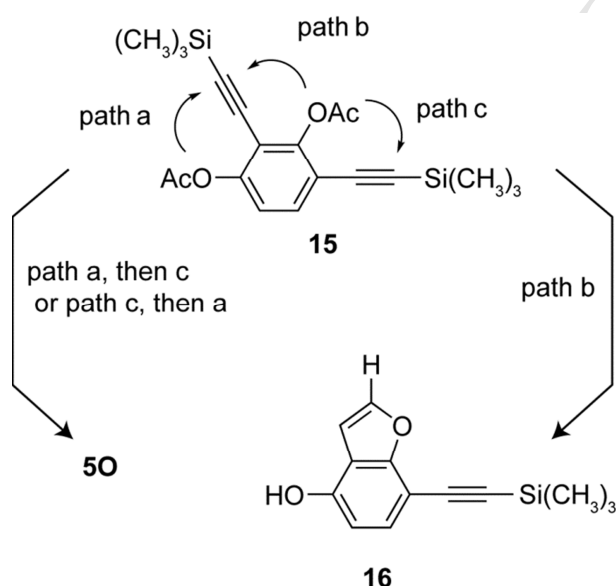


Figure 4. Plausible pathways for the cyclization of **15**.

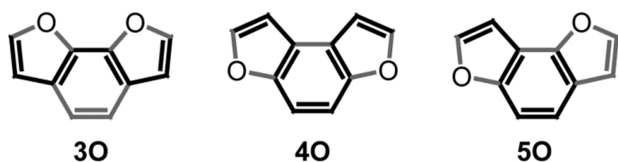
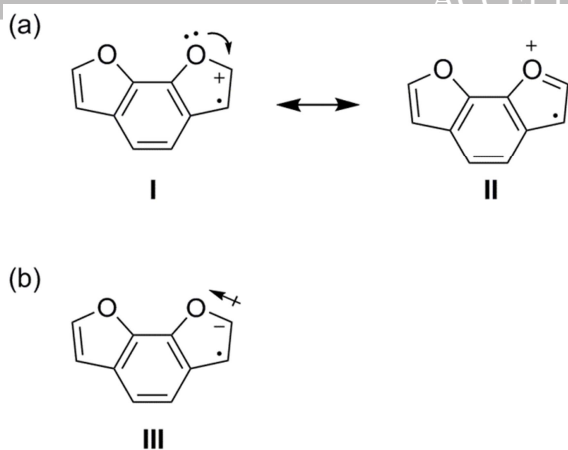


Figure 5. The longest series of alternating single and double bonds in **30–50** (black lines).



**Figure 6.** Principal canonical structures contributing to stabilization/destabilization of  $3\text{O}^+$  (a) and  $3\text{O}^-$  (b).

structure **II**). In the neutral state, the two oxygen atoms of **3O** would be slightly negative (i.e.,  $\delta^-$ ) because of their high electronegativity, which would lead to electrostatic repulsion between these two atoms. The extent of this repulsive interaction would be smaller in  $3\text{O}^+$  compared with **3O** because the  $\delta^-$  characteristics of the oxygen atoms would be diminished by resonance between canonical structures **I** and **II**, as shown in Figure 6. These effects would enhance the stability of  $3\text{O}^+$ , thereby raising the HOMO energy level of **3O**. This effect was not observed in **4O** because the oxygen atoms in this compound were not adjacent to each other.

A comparison of the LUMO energy levels of compounds **3O–5O** (i.e.,  $E_{\text{LUMO}}(\mathbf{3O}) > E_{\text{LUMO}}(\mathbf{5O}) > E_{\text{LUMO}}(\mathbf{4O})$ ) revealed that  $E_{\text{LUMO}}(\mathbf{3O})$  was higher than expected. This effect was attributed to the destabilizing effect of the radical anion state of **3O**,  $3\text{O}^-$ . Consideration of the different resonance forms of  $3\text{O}^-$  suggested that canonical structure **III** would make the greatest contribution to the overall structure, with the negative charge located on the  $\alpha$  position of the furan ring and the unpaired electron located at the  $\beta$  position. The close proximity of the oxygen atom next to the negatively charged carbon atom would most likely destabilize the system because of its strong  $\pi$ -donating character. However, the inductive effect of the oxygen atoms in canonical form **III** would also have a stabilizing effect on this structure. It is noteworthy that similar stabilization effects have been observed in methoxymethyl anions, where the conjugated acid, dimethyl ether, was found to be more acidic than the carbon analogue, propane.<sup>44</sup> The oxygen atoms in  $3\text{O}^-$  would have greater  $\delta^-$  character than those in **3O** because of the inductive effect (as depicted in **III**), which would lead a greater degree of electrostatic repulsion. Consequently,  $3\text{O}^-$  would be destabilized, which would lead to the observed increase in the LUMO energy level of **3O**. A similar process was also applied to develop a deeper understanding of the order of the HOMO and LUMO energy levels in **3S–5S** and **3Se–5Se** (See Supplementary data).

As mentioned above the LUMO energy levels of **1O–1Se** decreased in the order of  $E_{\text{LUMO}}(\mathbf{1O}) > E_{\text{LUMO}}(\mathbf{1S}) > E_{\text{LUMO}}(\mathbf{1Se})$ . Similar results were also observed following a comparison of the LUMO energy levels of **3O–3Se**, **4O–4Se** and **5O–5Se**, where the LUMO energy levels decreased in the order of  $\text{XO} > \text{XS} > \text{XSe}$ , where  $\text{X} = 3, 4$  and  $5$ . In contrast, there were considerable differences in the order of the LUMO energy levels of **2O–2Se**, where  $E_{\text{LUMO}}(\mathbf{2O}) > E_{\text{LUMO}}(\mathbf{2Se}) > E_{\text{LUMO}}(\mathbf{2S})$ . In all cases, the fused-furan compounds showed much lower electron-accepting characteristics than any of the other isomers, while electron-accepting characteristics of the fused-thiophene and fused-

selenophene compounds were comparable. The lower LUMO energy levels of the fused-thiophene and fused-selenophene compounds compared with the fused-furan compounds could be attributed to the stabilizing effects of the sulfur and selenium atoms in the radical anion states, as mentioned above.

In contrast to the LUMO energy levels, there were no obvious trends in the HOMO energy levels of **XO–XSe**, where  $\text{X} = 1–5$ . It was previously reported that the HOMO energy levels of **1O–1Se** and **2O–2Se** increased in the order of  $E_{\text{HOMO}}(\mathbf{1O}) < E_{\text{HOMO}}(\mathbf{1S}) < E_{\text{HOMO}}(\mathbf{1Se})$  and  $E_{\text{HOMO}}(\mathbf{2O}) < E_{\text{HOMO}}(\mathbf{2S}) < E_{\text{HOMO}}(\mathbf{2Se})$ , respectively.<sup>11</sup> Similar orders to these have also been observed following a comparison of the electron-donating characteristics of fused-furan compounds with their thiophene and selenophene analogues. For example, the vertical ionization energies measured by photoelectron spectroscopy for benzofuran, benzothiophene and benzoselenophene have been reported to be 8.37, 8.13 and 8.03 eV, respectively.<sup>51</sup> However, the HOMO energy levels of **3O–3Se** and **4O–4Se** showed different orders, which increased in the order of  $E_{\text{HOMO}}(\mathbf{3S}) < E_{\text{HOMO}}(\mathbf{3Se}) < E_{\text{HOMO}}(\mathbf{3O})$  and  $E_{\text{HOMO}}(\mathbf{4S}) < E_{\text{HOMO}}(\mathbf{4Se}) < E_{\text{HOMO}}(\mathbf{4O})$ , respectively. Fused-furan compounds are generally the most electron-donating of these systems, whereas fused-thiophene compounds are generally the least. In contrast, the order of the HOMO energy levels of **5O–5Se** was determined to be  $E_{\text{HOMO}}(\mathbf{5S}) < E_{\text{HOMO}}(\mathbf{5O}) < E_{\text{HOMO}}(\mathbf{5Se})$ , where the most electron-donating compound was no longer a fused-furan compound but a fused-selenophene compound instead, although the fused-furan compound was still more electron-donating than the thiophene compound. Since the gaps between the HOMO energy levels were generally small (0.01–0.09 eV), various factors should be intrinsically intertwined, resulting in the complicated ordering of the HOMO energy levels of these compounds.

#### 4. Conclusions

Compared with **1O** and **2O**, there were considerable differences in the electronic absorption and fluorescent spectra of compounds **3O–5O**. Furthermore, there were significant differences in the  $\Phi_{\text{F}}$  values of **3O–5O**, whereas those of **1O** and **2O** almost identical. The electron-donating characteristics of **3O–5O** increased in the order of  $\mathbf{5O} < \mathbf{3O} = \mathbf{4O}$  based on the results of CV measurements and DFT calculations. In contrast, their electron-accepting characteristics, which were estimated by DFT calculations, increased in the order of  $\mathbf{5O} < \mathbf{3O} < \mathbf{4O}$ . The differences in these orders have been successfully explained in terms of the differences in the length of the alternating single and double bonds in the canonical structures of these compounds. The stabilizing effects achieved through a reduction in the Coulombic repulsion in  $3\text{O}^+$ , as well as the destabilizing effects achieved by increasing the Coulombic repulsion in  $3\text{O}^-$  have also been discussed in detail. The orders of the HOMO and LUMO energy levels of **3S–5S** and **3Se–5Se** have been explained in a similar manner, although enhanced Coulombic repulsion effects would result in the destabilization of  $3\text{S}^+$  and  $3\text{Se}^+$ , whereas decreased Coulombic repulsion would result in the stabilization of  $3\text{S}^-$  and  $3\text{Se}^-$ . These results will provide important information for the design of electronic materials consisting of **3O–5O** moieties. Given that several **3S-**, **4S-** and **5S-** based polymers have shown enhanced properties compared with their **1S–2S** analogues, it is envisaged that compounds consisting of **3O–5O** moieties will provide better materials than their **1O–2O** analogues.

#### 5. Experimental details

##### 5.1. Synthesis

## 5.1.1. General

All commercially available chemicals were used without further purification except THF, which was distilled over benzophenone-ketyl before use.  $^1\text{H}$  and  $^{13}\text{C}$  NMR spectra were recorded on a JEOL JNM-ECP600 (600 MHz for  $^1\text{H}$  and 150 MHz for  $^{13}\text{C}$ ) with tetramethylsilane as internal reference. Mass spectra were conducted on a JEOL MStation JMS-700 (EI).

5.1.2. Synthesis of 2,3-diiodohydroquinone (**10**)

To a solution of 2,3-diiodo-1,4-benzoquinone<sup>52</sup> (0.15 g, 0.42 mmol) in chloroform (20 mL) was added an aqueous solution (15 mL) of sodium dithionite ( $\text{Na}_2\text{S}_2\text{O}_4$ ) (0.15 g, 0.83 mmol) dropwisely at ambient temperature in air. After stirring for 3 hours in dark, the reaction mixture was acidified by using 3 mol/L hydrochloric acid. The organic layer was separated, and the aqueous layer was extracted with chloroform. The combined chloroform solution was washed by burin, dried over anhydrous magnesium sulfate, then concentrated. The target compound **10** was obtained as a white powder (0.12 g, 81%). Mp 203–204 °C (dec).  $^1\text{H}$  NMR (acetone- $d_6$ ):  $\delta$  = 6.91 (s, 2H, ar), 2.86 (s, 2H, OH).  $^{13}\text{C}$  NMR (acetone- $d_6$ ):  $\delta$  = 157.79, 115.88, 99.56. MS:  $m/z$  = 362 ( $\text{M}^+$ ). HRMS ( $m/z$ ): 361.8301 ( $\text{M}^+$ , calcd. 361.8301 for  $\text{C}_6\text{H}_4\text{O}_2\text{I}_2$ ).

5.1.3. Synthesis of 2,3-diacetoxy-1,4-diiodobenzene (**7**)

To a mixture of 3,6-diiodocatechol **8**<sup>53</sup> (1.10 g, 3.01 mmol), acetic anhydride (9.0 mL, 95 mmol) and triethylamine (13 mL, 95 mmol) was added 4-dimethylaminopyridine (DMAP) (59 mg, 0.48 mmol) at ambient temperature in air. After stirring for 2 hours, iced water was added. The organic substrate was diluted with diethyl ether, washed with aqueous sodium bicarbonate (saturated), 3 mol/L hydrochloric acid and burin, and dried over anhydrous magnesium sulfate. Evaporation of the solvents gave a light brown solid, which was recrystallized from ethanol to yield the target compound **7** as colorless plates (1.21 g, 89 %). Mp 203–205 °C.  $^1\text{H}$  NMR ( $\text{CDCl}_3$ ):  $\delta$  = 7.44 (s, 2H, ar), 2.35 (s, 6H,  $\text{COCH}_3$ ).  $^{13}\text{C}$  NMR ( $\text{CDCl}_3$ ):  $\delta$  = 167.03, 144.42, 137.60, 91.87, 20.77. MS:  $m/z$  = 446 ( $\text{M}^+$ ). HRMS ( $m/z$ ): 445.8504 ( $\text{M}^+$ , calcd. 445.8512 for  $\text{C}_{10}\text{H}_8\text{O}_4\text{I}_2$ ). Compounds **11** and **14** were synthesized from **10** and 2,4-diiodoresorcinol **13**,<sup>54</sup> respectively, in similar manners.

**1,4-diacetoxy-2,3-diiodobenzene (11)**. Colorless needles. Yield 83%. Mp 182–184 °C.  $^1\text{H}$  NMR ( $\text{CDCl}_3$ ):  $\delta$  = 7.16 (s, 2H, ar), 2.37 (s, 6H,  $\text{COCH}_3$ ).  $^{13}\text{C}$  NMR ( $\text{CDCl}_3$ ):  $\delta$  = 168.34, 149.38, 122.92, 106.69, 21.45. MS:  $m/z$  = 446 ( $\text{M}^+$ ). HRMS ( $m/z$ ): 445.8505 ( $\text{M}^+$ , calcd. 445.8512 for  $\text{C}_{10}\text{H}_8\text{O}_4\text{I}_2$ ).

**1,3-Diacetoxy-2,4-diiodobenzene (14)**. Slightly brown powder. Yield 86%. Mp 77–79 °C.  $^1\text{H}$  NMR ( $\text{CDCl}_3$ ):  $\delta$  = 7.81 (d,  $J$  = 8.4 Hz, 1H, ar), 6.78 (d,  $J$  = 8.4 Hz, 1H, ar), 2.42 (s, 3H,  $\text{COCH}_3$ ), 2.37 (s, 3H,  $\text{COCH}_3$ ).  $^{13}\text{C}$  NMR ( $\text{CDCl}_3$ ):  $\delta$  = 168.06, 167.04, 152.91, 152.80, 139.05, 121.96, 89.23, 86.81, 21.38, 21.18. MS:  $m/z$  = 446 ( $\text{M}^+$ ). HRMS ( $m/z$ ): 445.8515 ( $\text{M}^+$ , calcd. 445.8512 for  $\text{C}_{10}\text{H}_8\text{O}_4\text{I}_2$ ).

5.1.4. Synthesis of 2,3-diacetoxy-1,4-bis(trimethylsilylethynyl)benzene (**8**)

A mixture of **7** (0.10 g, 0.23 mmol) and CuI (4.1 mg, 0.022 mmol) in diisopropylamine (10 mL) was degassed by purging with argon. After dichlorobis(triphenylphosphine)palladium (18 mg, 0.026 mmol) and trimethylsilylacetylene (0.10 mL, 0.98 mmol) were added, the reaction mixture was stirred at ambient temperature for 3 hours. After addition of water, organic layer was separated, and aqueous layer was extracted with ethyl acetate. Combined organic phase was washed with 3 mol/L hydrochloric acid and brine, dried over anhydrous magnesium

sulfate, and evaporated to dryness. The crude product was purified by column chromatography ( $\text{SiO}_2$ , 1:4 ethyl acetate-hexane) to yield the target compound **8** as a white powder (83.2 mg, 93%). Mp 112–114 °C.  $^1\text{H}$  NMR ( $\text{CDCl}_3$ ):  $\delta$  = 7.30 (s, 2H, ar), 2.31 (s, 6H,  $\text{COCH}_3$ ), 0.23 (s, 18H,  $\text{SiCH}_3$ ).  $^{13}\text{C}$  NMR ( $\text{CDCl}_3$ ):  $\delta$  = 167.33, 144.46, 129.82, 119.40, 102.37, 98.44, 20.39, –0.28. MS:  $m/z$  = 386 ( $\text{M}^+$ ). HRMS ( $m/z$ ): 386.1363 ( $\text{M}^+$ , calcd. 386.1370 for  $\text{C}_{20}\text{H}_{26}\text{O}_4\text{Si}_2$ ). Compounds **12** and **15** were synthesized from **11** and **14**, respectively, in similar manners.

**1,4-Diacetoxy-2,3-bis(trimethylsilylethynyl)benzene (12)**. A white powder. Yield 53%. Mp 94–96 °C.  $^1\text{H}$  NMR ( $\text{CDCl}_3$ ):  $\delta$  = 7.03 (s, 2H, ar), 2.32 (s, 6H,  $\text{COCH}_3$ ), 0.25 (s, 18H,  $\text{SiCH}_3$ ).  $^{13}\text{C}$  NMR ( $\text{CDCl}_3$ ):  $\delta$  = 168.39, 149.56, 122.76, 121.31, 104.83, 97.27, 20.77, –0.17. MS:  $m/z$  = 386 ( $\text{M}^+$ ). HRMS ( $m/z$ ): 386.1363 ( $\text{M}^+$ , calcd. 386.1370 for  $\text{C}_{20}\text{H}_{26}\text{O}_4\text{Si}_2$ ).

**1,3-Diacetoxy-2,4-bis(trimethylsilylethynyl)benzene (15)**. A yellow powder. Yield 48%. Mp 73–75 °C.  $^1\text{H}$  NMR ( $\text{CDCl}_3$ ):  $\delta$  = 7.43 (s,  $J$  = 8.4 Hz, 1H, ar), 6.97 (s,  $J$  = 8.4 Hz, 1H, ar), 2.33 (s, 3H,  $\text{COCH}_3$ ), 2.31 (s, 3H,  $\text{COCH}_3$ ), 0.23 (s, 9H,  $\text{SiCH}_3$ ), 0.23 (s, 9H,  $\text{SiCH}_3$ ).  $^{13}\text{C}$  NMR ( $\text{CDCl}_3$ ):  $\delta$  = 168.03, 167.33, 154.03, 152.25, 132.66, 119.82, 115.82, 113.10, 105.15, 100.12, 98.30, 93.96, 20.77, 20.39, –0.21, –0.24. MS:  $m/z$  = 386 ( $\text{M}^+$ ). HRMS ( $m/z$ ): 386.1379 ( $\text{M}^+$ , calcd. 386.1370 for  $\text{C}_{20}\text{H}_{26}\text{O}_4\text{Si}_2$ ).

5.1.5. Synthesis of benzo[1,2-*b*:6,5-*b'*]difuran (**30**)

A mixture of tetra-*n*-butylammonium fluoride (1 mol/L in THF, 4.2 mL, 4.2 mmol) and 4 Å molecular sieves (1.0 g) in THF (30 mL) was degassed by purging with argon and stirred at room temperature for 1 hour. Then a solution of **8** (0.54 g, 1.4 mmol) in THF (20 mL) was added and the whole was stirred at 60 °C for 12 hours. The suspension was cooled to room temperature, then water was added. The organic substrate was extracted with *n*-pentane. The combined organic phase was washed with 3 mol/L hydrochloric acid and brine, dried over anhydrous magnesium sulfate, and evaporated to dryness. The crude product was purified by column chromatography ( $\text{SiO}_2$ , *n*-pentane) to yield the target compound **30** as a colorless oil (77 mg, 35%).  $^1\text{H}$  NMR (600 MHz,  $\text{CDCl}_3$ ):  $\delta$  = 7.67 (d,  $J$  = 1.8 Hz, 2H, ar), 7.46 (s, 2H, ar), 6.90 (d,  $J$  = 1.8 Hz, 2H, ar).  $^{13}\text{C}$  NMR (150 MHz,  $\text{CDCl}_3$ ):  $\delta$  = 144.05, 140.05, 125.44, 116.11, 107.55. MS:  $m/z$  = 158 ( $\text{M}^+$ ). HRMS ( $m/z$ ): 158.0366 ( $\text{M}^+$ , calcd. 154.0368 for  $\text{C}_{10}\text{H}_6\text{O}_2$ ). Compounds **40** and **50** were synthesized from **12** and **15**, respectively, in similar manners.

**Benzo[1,2-*b*:4,3-*b'*]difuran (40)**. Yield 41%.  $^1\text{H}$  NMR ( $\text{CDCl}_3$ ):  $\delta$  = 7.73 (d,  $J$  = 1.8 Hz, 2H, ar), 7.46 (s, 2H, ar), 6.97 (d,  $J$  = 1.8 Hz, 2H, ar).  $^{13}\text{C}$  NMR ( $\text{CDCl}_3$ ):  $\delta$  = 151.62, 145.21, 119.87, 107.77, 105.54. MS:  $m/z$  = 158 ( $\text{M}^+$ ). HRMS ( $m/z$ ): 158.0364 ( $\text{M}^+$ , calcd. 154.0368 for  $\text{C}_{10}\text{H}_6\text{O}_2$ ).

**Benzo[1,2-*b*:3,4-*b'*]difuran (50)**. Yield 52%.  $^1\text{H}$  NMR ( $\text{CDCl}_3$ ):  $\delta$  = 7.67 (d,  $J$  = 1.8 Hz, 1H, ar), 7.66 (d,  $J$  = 1.2 Hz, 1H, ar), 7.49–7.44 (m, 2H, ar), 7.05 (s, 1H, ar), 6.87 (d,  $J$  = 1.8 Hz, 1H, ar).  $^{13}\text{C}$  NMR ( $\text{CDCl}_3$ ):  $\delta$  = 154.21, 147.71, 144.61, 143.78, 121.90, 116.65, 113.11, 107.41, 107.23, 102.98. MS:  $m/z$  = 158 ( $\text{M}^+$ ). HRMS ( $m/z$ ): 158.0372 ( $\text{M}^+$ , calcd. 154.0368 for  $\text{C}_{10}\text{H}_6\text{O}_2$ ).

## 5.2. Electron absorption/emission spectra

Electronic absorption spectra were acquired in cyclohexane and ethanol on a Shimadzu UV-2400PC spectrometer (Shimadzu, Kyoto, Japan). Fluorescent spectra were recorded in cyclohexane and ethanol on a Shimadzu RF-5300PC spectrometer using a 450 W xenon short arc and sample detection with a geometry of 90°. Fluorescence quantum yields were measured in ethanol using an absolute PL quantum yield measurement system consisting of a

JASCO FP-6600 spectrometer (JASCO, Tokyo, Japan) equipped with an integrating ILF-533 sphere. ferrocene/ferricinium redox couple ( $E^{1/2} = +0.46$  V), which was measured under the same conditions.

### 5.3. Electrochemical analyses

Cyclic voltammetry (CV) experiments were performed in 1 mM of substrate on an ALS-600a electrochemical analyzer (Bioanalytical Systems, Inc., West Lafayette, IN, USA). All of the oxidation CV measurements were conducted in anhydrous acetonitrile containing 0.1 M tetrabutylammonium hexafluorophosphate ( $n\text{Bu}_4\text{NPF}_6$ ) as a supporting electrolyte, which was purged with argon prior to the experiment. A platinum electrode was used as the working electrode with a platinum wire as the counter electrode. All of the potentials were recorded against an Ag/AgCl electrode, which was used as a reference electrode. The values were then calibrated against the standard

### 5.4. Theoretical studies

Our theoretical investigations of compounds **3O–5O**, **1S–5S** and **1Se–5Se** were performed on the optimized structures using density functional theory calculations at the B3LYP/6-31G(d,p) level with Spartan '04 for Windows (version 1.0.3, Wavefunction Inc., City, Country) on Microsoft Windows XP. Time-dependent DFT (TD-DFT) calculations were performed at the B3LYP/6-31G(d) level using the Gaussian 98 package.<sup>55</sup> The symmetries of the molecular structures were assumed to be  $C_{2v}$  (for **3O**, **4O**, **3S**, **4S**, **3Se** and **4Se**) and  $C_s$  (for **5O**, **5S** and **5Se**) for all of the calculations, because the molecules bearing lower symmetries were energetically less favorable.

## Acknowledgments

This work was supported by JSPS KAKENHI Grant Number 24550151.

## References and notes

- (a) Klauk, H., Ed.; *Organic Electronics: Materials, Manufacturing and Applications*; Wiley-VCH: Weinheim, Germany, 2006. (b) Klauk, H., Ed.; *Organic Electronics II: More Materials and Applications*; Wiley-VCH: Weinheim, Germany, 2012. (c) Wang, C.; Dong, H.; Hu, W.; Liu, Y.; Zhu, D. *Chem. Rev.* **2012**, *112*, 2208–2267.
- Katritzky, A. R.; Ramsden, C. A.; Joule, J. A.; Zhdankin, V. V. *Handbook of Heterocyclic Chemistry, 3rd Ed.*; Elsevier: Amsterdam, The Netherlands, 2000.
- Handbook of Thiophene-Based Materials: Applications in Organic Electronics and Photonics, Ed. by Perepichka, I. F.; Perepichka, D. F., Wiley: Chichester, UK, 2009.
- Bleiholder, C.; Gleiter, R.; Werz, D. B.; Köppel, H. *Inorg. Chem.* **2007**, *46*, 2249–2260.
- Bleiholder, C.; Werz, D. B.; Köppel, H.; Gleiter, R. *J. Am. Chem. Soc.* **2006**, *128*, 2666–2674.
- Liu, Y.; Di, C.-a.; Du, C.; Liu, Y.; Lu, K.; Qiu, W.; Yu, G. *Chem. Eur. J.* **2010**, *16*, 2231–2239.
- Jiang, W.; Zhou, Y.; Geng, H.; Jiang, S.; Yan, S.; Hu, W.; Wang, Z.; Shuai, Z.; Pei, J. *J. Am. Chem. Soc.* **2011**, *133*, 1–3.
- Rieger, R.; Beckmann, D.; Pisula, W.; Steffen, W.; Kastler, M.; Müllen, K. *Adv. Mater.* **2010**, *22*, 83–86.
- Ramírez-Solís, A.; Bernal-Jaquez, R.; Zicovich-Wilson, C. M. *Chem. Phys. Lett.* **2014**, *607*, 47–51.
- Bronstein, H.; Chen, Z.; Ashraf, R. S.; Zhang, W.; Du, J.; Durrant, J. R.; Tuladhar, P. S.; Song, K.; Watkins, S. E.; Geerts, Y.; Wienk, M. M.; Janssen, R. A. J.; Anthopoulos, T.; Sirringhaus, H.; Heeney, M.; McCulloch, I. J. *J. Am. Chem. Soc.* **2011**, *133*, 3272–3275.
- Ye, L.; Zhang, S.; Huo, L.; Zhang, M.; Hou, J. *Acc. Chem. Res.* **2014**, *47*, 1595–1603.
- Liu, M.; Rieger, R.; Li, C.; Menges, H.; Kastler, M.; Baumgarten, M.; Müllen, K. *ChemSusChem* **2010**, *3*, 106–111.
- Rieger, R.; Beckmann, D.; Mavrin, A.; Kastler, M.; Müllen, K. *Chem. Mater.* **2010**, *22*, 5314–5318.
- Huang, P.; Du, J.; Biewer, M. C.; Stefan, M. C. *J. Mater. Chem. A* **2015**, *3*, 6244–6257.
- Santos-Pérez, J.; Crespo-Hernández, C. E.; Reichardt, C.; Cabrera, C. R.; Feliciano-Ramos, I.; Arroyo-Ramírez, A.; Meador, M. A. *J. Phys. Chem. A* **2011**, *115*, 4157–4168.
- Mitsui, C.; Tanaka, H.; Tsuji, H.; Nakamura, E. *Chem. Asian J.* **2011**, *6*, 2296–2300.
- Tsuji, H.; Mitsui, C.; Ilies, L.; Sato, Y.; Nakamura, E. *J. Am. Chem. Soc.* **2007**, *129*, 11902–11903.
- Yi, C.; Blum, C.; Lehmann, M.; Keller, S.; Liu, S.-X.; Frei, G.; Neels, A.; Hauser, J.; Schürch, S.; Decurtins, S. *J. Org. Chem.* **2010**, *75*, 3350–3357.
- Shukla, R.; Wadumethrige, S. H.; Lindeman, S. V.; Rathore, R. *Org. Lett.* **2008**, *10*, 3587–3590.
- Hayashi, N.; Y. Saito; Higuchi, H.; Suzuki, K. *J. Phys. Chem. A* **2009**, *113*, 5342–5347.
- Wex, B.; Kaafarani, B. R.; Danilov, E. O.; Neckers, D. C. *J. Phys. Chem. A* **2006**, *110*, 13754–13758.
- Zhang, K.; Tieke, B.; Forgie, J. C.; Vilela, F.; Skabara, P. J. *Macromolecules* **2012**, *45*, 743–750.
- Nielsen, C. B.; Brock-Nannestad, T.; Reenberg, T. K.; Hammershøj, P.; Christensen, J. B.; Stouwdam, J. W.; Pittelkow, M. Organic Light-Emitting Diodes from Symmetrical and Chem. *Eur. J.* **2010**, *16*, 13030–13034.
- Huong, V. T. T.; Tai, T. B.; Nguyen, M. T. *RSC Advances* **2015**, *5*, 24167–24174.
- Vestweber, H.; Heil, H.; Stoessel, P.; Buesing, A.; Parham, A.; Fortte, R. PCT Int. Appl. (2006), WO 2006122630.
- Kato, T.; Numata, M.; Nishimura, K.; Iwakuma, T.; Hosokawa, C.; Yoshida, K. PCT, Int. Appl. (2009), WO 2009148062.
- Gaussian 98, Revision A.11.1. M. J. Frisch, G. W. Trucks, H. B. Schlegel, G. E. Scuseria, M. A. Robb, J. R. Cheeseman, V. G. Zakrzewski, J. A. Montgomery, Jr., R. E. Stratmann, J. C. Burant, S. Dapprich, J. M. Millam, A. D. Daniels, K. N. Kudin, M. C. Strain, O. Farkas, J. Tomasi, V. Barone, M. Cossi, R. Cammi, B. Mennucci, C. Pomelli, C. Adamo, S. Clifford, J. Ochterski, G. A. Petersson, P. Y. Ayala, Q. Cui, K. Morokuma, P. Salvador, J. J. Dannenberg, D. K. Malick, A. D. Rabuck, K. Raghavachari, J. B. Foresman, J. Cioslowski, J. V. Ortiz, A. G. Baboul, B. B. Stefanov, G. Liu, A. Liashenko, P. Piskorz, I. Komaromi, R. Gomperts, R. L. Martin, D. J. Fox, T. Keith, M. A. Al-Laham, C. Y. Peng, A. Nanayakkara, M. Challacombe, P. M. W. Gill, B. Johnson, W. Chen, M. W. Wong, J. L. Andres, C. Gonzalez, M. Head-Gordon, E. S. Replogle, and J. A. Pople, Gaussian, Inc., Pittsburgh PA, 2001.
- Schaeffer, H. J.; Vince, R. *J. Org. Chem.* **1963**, *28*, 1653–1656.
- Royer, R.; Bisagni, E.; Hudry, C.; Cheutin, A.; Desvoye, M. L. *Bull. Soc. Chim. Fr.* **1963**, 1003–1007.
- Rene, L.; Buisson, J. P.; Royer, R.; Dietrich, A. *Eur. J. Med. Chem.* **1978**, *13*, 435–439.
- Kellogg, R. M.; Groen, M. B.; Wynberg, H. *J. Org. Chem.* **1967**, *32*, 3093–3100.
- Loader, C. E.; Timmons, C. J. Photochemistry, V. *J. Chem. Soc. Sect. C* **1967**, 1677–1681.
- Cagniant, P.; Kirsch, G. C. *R. Acad. Sci., Ser. C* **1976**, *282*, 465–468.
- Glenn, R. W.; Lim, M.; Gardlik, J. M.; Jones, S. D.; Murphy, B. P.; Rees, C. W. U. S. Pat. US20050193504.
- Sonogashira, K.; Tohda, Y.; Hagihara, N. *Tetrahedron Lett.* **1975**, *50*, 4467–4470.
- Hennrich, G. *Tetrahedron* **2004**, *60*, 9871–9876.
- Ito, Y.; Aoyama, T.; Shioiri, T. *Synlett* **1997**, 1163–1164.
- Brusso, J. L.; Hirst, O. D.; Dadvand, A.; Ganesan, S.; Ciccoira, F.; Robertson, C. M.; Oakley, R. T.; Rosei, F.; Perepichka, D. F. *Chem. Mater.* **2008**, *20*, 2484–2494.
- Tsuji, H.; Shoyama, K.; Nakamura, E. *Chem. Lett.* **2012**, *41*, 957–959.
- Nonell, S.; Ferreras, L. R.; Cañete, A.; Lemp, E.; Günther, G.; Pizarro, N.; Zanocco, A. L. *J. Org. Chem.* **2008**, *73*, 5371–5378.
- Handbook of Photochemistry, 3rd Ed.*, Ed. by Montaliti, M.; Credi, A.; Prodi, L.; Gandolfi, M. T., CRC Press, Boca Raton, USA, 2006.
- Pomrèhne, J.; Vestweber, H.; Guss, W.; Mahrt, R. F.; Bässler, H.; Porsch, M.; Daub, J. *Adv. Mater.* **1995**, *7*, 551–554.
- Coropceanu, V.; Kwon, O.; Wex, B.; Kaafarani, B. R.; Gruhn, N. E.; Durivage, J. C.; Neckers, D. C.; Brédas, J.-L. *Chem. Eur. J.* **2006**, *12*, 2073–2080.
- Koopmans, T. *Physica* **1934**, *1*, 104–113.
- Bernasconi, C. F.; Kittredge, K. *J. Org. Chem.* **1998**, *63*, 1944–1953.
- Ref 2; p 124.
- Hammershøj, P.; Reenberg, T. K.; Pittelkow, M.; Nielsen, C. B.; Hammerich, O.; Christensen, J. B. *Eur. J. Org. Chem.* **2006**, 2786–2794.
- Zhu, Z.; Swager, T. M. *Org. Lett.* **2001**, *3*, 3471–3474.
- Weitl, F. L. *J. Org. Chem.* **1976**, *41*, 2044–2045.

## Supplementary Material

Discussion on the HOMO/LUMO energy levels of **3S–5S** and **3Se–5Se**, supplementary data (electronic absorption and fluorescence spectra of **3O**, **4O** and **5O** in EtOH, the HOMO and LUMO orbitals of **3O–5O**, **3S–5S** and **3Se–5Se** and the HOMO–1, HOMO, LUMO and LUMO+1 energy levels obtained by B3LYP/6-31G(d,p) calculations, and <sup>1</sup>H and <sup>13</sup>C NMR spectra of **3O–5O**, **7**, **8**, **10–12**, **14** and **15** can be found at <http://dx.doi.org/...>